RESEARCH ARTICLE

The effect of chronic neuroglycopenia on resting state networks in GLUT1 syndrome across the lifespan

Anna Elisabetta Vaudano[1,2] [ID] | Sara Olivotto[3] | Andrea Ruggieri[2] |
Giuliana Gessaroli[1] | Francesca Talami[2] | Antonia Parmeggiani[4,5] |
Valentina De Giorgis[6] | Pierangelo Veggiotti[3] | Stefano Meletti[1,2]

[1]Neurology Unit, OCSAE Hospital, AOU Modena, Modena, Italy

[2]Department of Biomedical, Metabolic, and Neural Sciences, University of Modena and Reggio Emilia, Modena, Italy

[3]Pediatric Neurology Unit, V. Buzzi Hospital, University of Milan, Milan, Italy

[4]Child Neurology and Psychiatry Unit, Policlinico S. Orsola-Malpighi, Bologna, Italy

[5]Department of Medical and Surgical Sciences, University of Bologna, Italy

[6]Brain and Behavior Department, University of Pavia, Pavia, Italy

Correspondence
Anna Elisabetta Vaudano, Department of Biomedical, Metabolic, and Neural Science, University of Modena and Reggio Emilia, OCSAE Hospital, Via Giardini 1355, 41126 Modena, Italy.
Email: annavaudano@gmail.com

Abstract

Glucose transporter type I deficiency syndrome (GLUT1DS) is an encephalopathic disorder due to a chronic insufficient transport of glucose into the brain. PET studies in GLUT1DS documented a widespread cortico-thalamic hypometabolism and a signal increase in the basal ganglia, regardless of age and clinical phenotype. Herein, we captured the pattern of functional connectivity of distinct striatal, cortical, and cerebellar regions in GLUT1DS (10 children, eight adults) and in healthy controls (HC, 19 children, 17 adults) during rest. Additionally, we explored for regional connectivity differences in GLUT1 children versus adults and according to the clinical presentation. Compared to HC, GLUT1DS exhibited increase connectivity within the basal ganglia circuitries and between the striatal regions with the frontal cortex and cerebellum. The excessive connectivity was predominant in patients with movement disorders and in children compared to adults, suggesting a correlation with the clinical phenotype and age at fMRI study. Our findings highlight the primary role of the striatum in the GLUT1DS pathophysiology and confirm the dependency of symptoms to the patients' chronological age. Despite the reduced chronic glucose uptake, GLUT1DS exhibit increased connectivity changes in regions highly sensible to glycopenia. Our results may portrait the effect of neuroprotective brain strategy to overcome the chronic poor energy supply during vulnerable ages.

KEYWORDS

basal ganglia, cerebellum, children, functional connectivity, GLUT1DS, neuroglycopenia, striatum

1 | INTRODUCTION

Glucose is the principal source of energy for the brain. Glucose uptake by the brain cells is mediated by the transporter protein GLUT1.

GLUT1 is encoded by the gene SLC2A1 on chromosome 1p35-31.3 (Klepper 2008). Mutation of this gene evolves into a rare metabolic disorder named Glucose transporter type I deficiency syndrome (GLUT1DS; De Giorgis & Veggiotti, 2013; De Vivo et al., 1991;

Pearson, Akman, Hinton, Engelstad, & De Vivo, 2013; Verrotti, D'Egidio, Agostinelli, & Gobbi, 2012). Patients with classic GLUT1DS suffer low brain glucose levels and exhibit a phenotype characterized by early-onset seizures, development delay, microcephaly and a complex movement disorder (MD) combining features of paroxysmal ataxia and dystonia (Klepper 2012; Pearson, Akman, Hinton, Engelstad, & De Vivo, 2013). The laboratory hallmark of GLUT1DS is a low concentration of glucose in the cerebrospinal fluid (CSF), also known as hypoglycorrhachia (Leen et al., 2013). The GLUT1 defect can be confirmed by a functional in vitro assay that measure glucose uptake in the erythrocytes (Yang et al., 2011) and by mutation analysis of the SLC2A1 gene (Brockmann et al., 2001; De Giorgis et al., 2015). A precocious and correct diagnosis of this condition is noteworthy as the treatment with ketogenic diet (KD) dramatically improves symptoms and may also affect long-term outcome (Alter et al., 2015; Bertoli et al., 2014; Klepper, Engelbrecht, Scheffer, van der Knaap, & Fiedler, 2007; Ramm-Pettersen et al., 2013).

Since the first description of two children affected by GLUT1DS in 1991 (De Vivo et al., 1991), the knowledge of phenotypic spectrum of this condition has grown enormously (Hully et al., 2015). Milder phenotypes have been increasingly recognized and these includes generalized epilepsies (Arsov et al., 2012; Roulet-Perez, Ballhausen, Bonafé, Cronel-Ohayon, & Maeder-Ingvar, 2008; Striano et al., 2012), paroxysmal exercise-induced dyskinesia (PED; Suls et al., 2008; Suls et al., 2009), dystonic tremor and hemolytic anemia (De Giorgis & Veggiotti, 2013). In contrast to other neurometabolic conditions, GLUT1DS is not a progressive neurodegenerative disorder (Alter et al., 2015; Pascual, Van Heertum, Wang, Engelstad, & De Vivo, 2002). Most of the clinical manifestation of GLUT1DS occurs in age-dependent manner with highest symptoms load in early life becoming more muted in adulthood (Alter et al., 2015). Longitudinal studies in GLUT1DS have shown that while epilepsy is more prominent and disabling in infancy and childhood, patients often became seizure-free by adulthood, irrespective of antiepileptic treatment or KD (Leen et al., 2014). By contrast, dystonia and other paroxysmal (MDs), particularly PED, tend to develop later in childhood or during adolescence with variable progression throughout life (Alter et al., 2015; Leen et al., 2014).

Previous PET studies in GLUT1DS patients have shown a stable impairment of glucose uptake over a wide cortical-striatal-thalamic network from ages 19 months to 31 years old, indicating permanence of the metabolic footprint throughout life (Pascual et al., 2007; Pascual, Van Heertum, Wang, Engelstad, & De Vivo, 2002). Especially, dysfunction of basal ganglia circuits could be a key player in the generation of the complex MDs (especially PED; Suls et al., 2008), while cortico-thalamic dysfunction is implicated in the genesis of spike and wave complexes and epilepsy (Akman et al., 2015; Vaudano et al., 2017).

Resting-state functional magnetic resonance imaging (RSN FC-MRI) has been widely used to investigate brain connectivity and networks that exhibit correlated fluctuations in spontaneous brain activity (Azeez & Biswal, 2017). This activity is high energy demanding, consuming up to 80% of the cerebral glucose and serves to support synaptic transmission and to sustain the resting potentials in neurons and glia (Attwell & Laughlin, 2001; Logothetis, Pauls, Augath, Trinath, & Oeltermann, 2001). Using a PET-MRI multimodal approach, it has been demonstrated a linear association between baseline measures of absolute glucose metabolism, a direct marker of neuronal activity, and the amplitude of the MRI signal fluctuations of the brain regions at rest (Tomasi, Wang, & Volkow, 2013). Thus, signal fluctuations with larger amplitudes were localized in brain regions characterized by higher metabolism. Despite recording different aspects of neural activity, similar RSNs were detected in fMRI and 18F-FDG data. These results argue for the common neural substrate of RSNs and encourage testing of the clinical utility of resting-state connectivity data (Savio et al., 2017). In this work, we aim to infer the FC-MRI of subcortical and cortical networks in patients with GLUT1DS compared to healthy controls. Based on previous evidences, we hypothesize that GLUT1DS shows an altered functional connectivity (FC) of the basal ganglia networks compared to controls. Similarly, given the chronic reduced glucose brain supply, we speculate a decrease in BOLD synchronization between high-level metabolic cortical regions (like visual cortex and precuneus) and the rest of the brain. Finally, we evaluate if the altered patterns of connectivity are different according to the clinical phenotype and in children with respect to adults in order to confirm the non-progressive course of this disorder and reveal potential new targets of intervention in vulnerable ages.

2 | METHODS

2.1 | Participants

Eighteen Italian right-handed GLUT1DS patients (mean age at fMRI: 19.22 ± 11.79 years; range 6–43 years; 12 females) were enrolled from September 2012 to March 2015 and underwent a VideoEEG-fMRI protocol. Of those, 10 patients were children (mean age at fMRI 10.6 ± 2.9 years; range 6–15) and eight adults (mean age at fMRI 29.6 ± 9.8 years; range 18–43). The recruited subjects fulfilled the clinical criteria for diagnosis of GLUT1DS (Pearson, Akman, Hinton, Engelstad, & De Vivo, 2013) and all but one presented pathogenic mutations in SLC2A1 gene (Table 1). The clinical, genetic, and molecular features of this GLUT1DS cohort have been described in detail in our previous paper (Vaudano et al., 2017). All patients except two cases (Pt #6 and Pt #18) had epileptic seizures throughout the disease course, mainly represented by absence seizures. MDs were documented in 13 patients, consisting in PED in all of them except one (Pt #4) who presented ataxia. Table S1 summarizes the clinical features of the GLUT1DS population at the time of the EEG-fMRI protocol. The mean time between the diagnosis and the EEG-fMRI experimental session was 2.9 ± 3.6 years (range 0–11 years).

A group of 36 healthy subjects (19 children, mean age 12.05 ± 2.5 years; 17 adults, mean age 31.74 ± 7.6 years) served as controls and underwent to a VideoEEG-fMRI study, using an identical protocol then GLUT1DS. Development, neurological status, and MRI scan were normal in all controls.

TABLE 1 Clinical feature and genetic of GLUT1 patients

Pt. ID	Age at diagnosis (yrs)/sex	Glycorrhachia (mg/dl)	CSF/plasma glucose ratio	Protein mutation	Sporadic/ familiar	Seizure type	Seizure onset (m)	MD	MD onset (m)	IQ
1	6/M	35	0.54	c1457delG_1 delG SPL	S	GTC, AS	11	PED, Dy	36	75
2	10/F	33	0.34	R126C	S	Myo, AS	30	PED, Dy	72	44
3	11/M	44	0.51	R223W	S	FS	11	PED, Cho	36	75
4	5/F	31	0.39	R153C	F	GTC, AS	12	A	16	104
5	10/M	40	0.47	R458W	F	FS	40	PED, Cho	60	85
6	10/F	33	0.38	V165I	F	/	/	PED, Dy, Cho	72	66
7	7/F	32	0.35	N34S	F	AS	24	/	/	76
8	9/F	34	0.38	R400C	S	AS, Myo	36	PED, Dy	36	50
9	5/F	40	0.41	Not found	S	Myo, GTC	39	/	/	112
10	20/F	31	0.38	R126C	S	AS, FS Myo	8	PED, A	18	60
11	14/F	40	0.44	P36R	S	AS	18	/	/	53
12	17/M	46	0.54	R458W	S	FS	60	PED, Dy	132	57
13	43/F	N/A	N/A	R458W	F	AS	72	/	/	78
14	29/F	41	0.44	V165I	F	AS, GTC	12	PED	N/A	55
15	24/F	N/A	N/A	V165I	F	AS	72	/	/	76
16	19/F	38	0.5	1166delV	S	AS	48	PED, Dy	7	80
17	39/M	42	0.43	N34S	F	AS	48	PED, Dy	N/A	75
18	15/M	44	0.44	R400H	S	/	/	PED, Dy	15	56

Note: Missense mutations were observed in the majority; case #1 and *n* #16 presented deletions. Amino acid mutations are represented by (capital) native amino acid (in one-letter code), amino acid number, and mutant amino acid. Nucleotide deletions are indicated by nucleotide number, del for deletion, nucleotide, or by native nucleotide, number, and mutant nucleotide.

Abbreviations: A, ataxia; AS, absences seizures; Cho, chorea; Dy, dystonia; F, female; F, familiar; FS, focal seizures; GTC, generalized tonic clonic seizures; IQ, intelligent quotient; m, months; M, male; MD, movement disorder; Myo, myoclonic seizures; N/A, not available; PED, paroxysmal exercise-induced dyskinesia; S, sporadic; yrs, years.

The human ethic committee of the University of Modena and Reggio Emilia approved this study and written informed consent was obtained from all the patients recruited or from their parents if underage.

2.2 | VideoEEG-fMRI protocol and analysis

2.2.1 | EEG-fMRI data acquisition

Patients and controls underwent a multimodal neuroimaging protocol that included Video and EEG acquired simultaneously to the fMRI acquisitions. Prior to in-magnet EEG recording, 10 min out-of magnet EEG was collected in a room adjacent to the scanner. Foam pads were used to help secure the EEG leads, minimize motion, and improve the subject's comfort. The patients and controls were constantly observed and recorded by means of a small camcorder positioned on the head coil inside the scanner pointing to the subject's face to obtain a split-screen video-documentation during the fMRI recording. Video and EEG were recorded synchronously with an online display. While FC analyses were performed on fMRI data, simultaneous EEG and Video recordings were of importance for the following reasons: (a) verify the occurrence of epileptiform activity during fMRI data acquisition; (b) check the vigilance fluctuations and recognize the occurrence of

sleep elements and stages; and (c) monitor the subjects' behavior while scanning especially regarding seizures' occurrence in patients and/or face and head movements.

We collected a 8 min rest scan comprising 240 echo planar imaging functional volumes (TR = 2.000 ms; TE = 35 ms; in-plane matrix = 64 × 64; voxel size: 4 × 4 × 4) with continuous simultaneous EEG recording. A high-resolution three-dimensional (3D) T1-weighted anatomic image has been acquired to allow accurate anatomic localization of BOLD increases/decreases. The volume consisted of 170 sagittal slices (TR = 9.9 ms; TE = 4.6 ms; in plane matrix = 256 × 256 × 170; voxel size = 1 × 1 × 1 mm; field of view = 240 mm).

All recordings were performed in the early afternoon. Subjects lied in a quite dimly lightened room and were asked to rest with eyes closed, do not sleep, and keep still during experimental sessions. No tasks were performed during the VideoEEG-fMRI acquisitions. Sedation was never used.

2.2.2 | EEG data analysis

After offline correction of the gradient artifacts and filtering of the EEG signal (Allen, Josephs, & Turner, 2000), the EEG data were

reviewed and preprocessed according to our previous published method (Avanzini et al., 2014; Vaudano et al., 2017). Briefly, scalp EEG has been recorded by means of a 32-channel MRI-compatible EEG recording system (Micromed, Mogliano Veneto, Italy). Electrodes were placed according to conventional 10–20 locations. ECG was recorded from two chest electrodes. The correction of the gradient artifact was performed offline by means of the Brain Quick System Plus software (Micromed, Mogliano Veneto, Italy; Allen, Josephs, & Turner, 2000). The EEG data were then exported in the .edf format and reviewed and analyzed by means of the BrainVision Analyzer 2.0 software (Brain Products, Munich, Germany). A band-pass filter between 1 and 70 Hz was applied to the continuous recording and channels showing high impedance or electrode displacement artifacts were interpolated through a cubic spline. Pulse-related artifacts were removed offline using the EEG processing package of Brain Analyzer (Allen, Polizzi, Krakow, Fish, & Lemieux, 1998).

The preprocessed EEG data were then submitted to an independent component analysis (ICA; Bell & Sejnowski, 1995; Makeig, Debener, Onton, & Delorme, 2004). For each participant, the 30 EEG channels signal was decomposed into 30 components (between F0 and F29) In patient populations, two experienced electroencephalographers (A.E.V., P.V.) reviewed both the standard EEG recordings and the relative individual components of the ICA-processed to identify the presence of interictal epileptiform activity (IED). After identification, IED were manually marked on EEG and exported as single event or variable-length blocks depending on their duration observed by EEG. The resulted text file was transformed in .mat file using a dedicated home-made script. Finally, these files were uploaded as first level covariates in the conn toolbox and regressed out during denoising steps.

2.2.3 | fMRI data preprocessing and analysis

Data analysis was performed using Statistical Parametric Mapping (SPM) version 12 (http://www.fil.ion.ucl.ac.uk/spm/software/spm12), in addition to the Functional Connectivity (CONN) toolbox (version 18.a, http://web.mit.edu/swg/software.htm). Preprocessing steps included: (a) slice timing correction for interleaved acquisition; (b) 3D motion correction; (c) reorienting both functional and structural images and then co-registering 3DT1 image to the mean functional image of each subject; (d) segmentation of 3DT1 images into gray matter, white matter (WM), and CSF tissue based on the Montreal Neurological Institute 152 (MNI152) stereotaxic space (2 mm^3); (e) spatial normalization by using the parameters from the segmentation procedure in each subject; and (f) spatial smoothing with a 8-mm full-width-at-half-maximum Gaussian kernel. Being the investigated population with children, to address concerns about age/related errors in registration (Wilke, Schmithorst, & Holland, 2003), we conducted secondary analysis in data registered to age dependent template and specifically we adopted the asymmetric T1 version of NIHPD atlas (age range 4.5–8.5 and 7.5–13 years old; Fonov et al., 2011; http://www.bic.mni.mcgill.ca/ServicesAtlas/NIHPD-obj1; see Data S1).

Each participant's preprocessed volume was regressed on principal components (PCs) extracted from subject-specific WM and CSF mask (five PC parameters) using a component based noise correction method (CompCor; Behzadi, Restom, Liau, & Liu, 2007) as well as six head motion parameters generated from SPM realignment of the concatenated time series (x, y, z, translation and pitch, yaw and roll rotation). Excessive motion was defined as more than 2.5 mm of translation and 2.5° of rotation in any direction. This level of censoring has been reported previously (Cao et al., 2009; Di Martino et al., 2011). CompCor addresses the confounding effects of subject movement without affecting intrinsic FC (Chai, Castañón, Ongür, & Whitfield-Gabrieli, 2012), thus global signal was not regressed. In addition, IED when present in GLUT1DS patients' group by EEG analysis and inspection, were included in the model as effect of no interest. Finally, functional data were band-pass filtered to 0.01–0.1 Hz to reduce the influence of noise. We then performed a seed-to-voxel analysis (bivariate correlation), using the group-defined region of interest (ROI) to generate whole-brain beta maps for each individual's (patients and controls) resting state runs. Specifically, the following bilateral ROI were selected: caudate, putamen, globus pallidus, thalamus, primary motor cortex, calcarine cortex, precuneus, and cerebellum. All the ROI were defined based on the automated anatomical labeling (AAL) template (Tzourio-Mazoyer et al., 2002) as implemented in the conn toolbox. Related to the cerebellar ROI, each of the 26 cerebellar regions distinguished by the AAL template was assigned to one of the two cerebellar regions of interest (hemisphere and vermis). In each subject, seeds' location was verified by superimposing each ROI on individual spatially normalized 3D images and it was checked that the seed does not exceed the boundary of the selected ROI. The rationale for choosing basal ganglia, thalamic, motor and cerebellar regions were based on the available literature on their presumed involvement by PET studies and clinical observation of MDs (Akman et al., 2015; Pascual, Van Heertum, Wang, Engelstad, & De Vivo, 2002, Pascual et al., 2007; Vaudano et al., 2017) while the PCU and visual cortex were selected as presumed to be regions of high-level of glucose consumption (Ishibashi, Sakurai, Shimoji, Tokumaru, & Ishii, 2018; Shokri-Kojori et al., 2019; Tomasi, Wang, & Volkow, 2013). After the toolbox had calculated the connectivity for each individual subject, second-level analyses were performed in order to reveal seed-based connectivity differences. Consistent with prior studies (Vincent et al., 2006; Vincent, Kahn, Snyder, Raichle, & Buckner, 2008), for networks with bilateral ROI seeds, the connectivity maps derived from the left and right ROI were averaged to create a single connectivity map. Comparisons were obtained by a two-way ANOVA with 2 (patients and controls) × 2 (children and adults) design in the SPM12 toolbox. After analyzing the main effect of group (patients vs. controls) and of age (children vs. adults), post hoc analyses were conducted to explore the following comparisons: (a) children with GLUT1DS versus healthy children; (b) adults with GLUT1DS versus healthy adults; and (c) children with GLUT1DS versus adults with GLUT1DS.

For both within and between group(s) analyses, the connectivity maps generated for each network were thresholded at the whole-

brain cluster-level FWE (family-wise error) corrected alpha level .05 for voxel-wise $p = .001$ to show regions correlated (positively and negatively) with the seed ROI. We also included age (at fMRI) and sex as covariates for all connectivity analyses to control for group differences in these variables on the regression coefficients.

Finally, to investigate the relationship between connectivity differences and clinical variables in the GLUT1DS population, we conducted whole brain multiple regression analysis to examine the linear relation between ROIs FC and the following measures: (a) age at diagnosis; (b) seizure's onset age; (c) intelligence quotient-IQ; (d) glycorrhachia; and (e) MD's onset age.

3 | RESULTS

3.1 | Data quality

No patients were excluded from further analyses due to excessive motion and sleep stages were not recorded in any patients/controls by simultaneous EEG inspection. Estimates of fMRI motion parameters were not different between groups: the average value of motion variables in the GLUT1DS population was equal to 0.074, while in Controls was 0.079 with no significant difference (one-way ANOVA, $p = .54$). In addition, we did not observe any correlation between nuisance variables and age at EEG-fMRI scan ($p = .88$). To ensure that the FC data were not contaminated by motion-based artifact in the BOLD signal, we tested for a motion dependence on the correlation between the data and motion quality control (QC) measures as well as the relationship between QC-FC and Euclidian distance between ROI pairs (Ciric et al., 2017) for both patients and controls. Absolute QC-FC for patients was $r = 0.04 \pm 0.16$, for controls was $r = -0.04 \pm 0.16$, while for patients adults was 0.01 ± 0.15 and for patients children was 0.03 ± 0.18. The QC-FC-distance dependent effects for patients ($r = .07$) and control ($r = .04$) outperformed almost all motion correction procedures reported by Ciric and colleagues (Ciric et al., 2017), suggesting the distance between ROI and the strength of FC was not contaminated by motion. EEG during fMRI revealed IED in 10 GLUT1 patients (#3, #5, #6, #9, #11, #17) constituted

by focal or generalized spike-and-wave discharges (SWD). These were treated as confounds as reported in Section 2.

3.2 | Connectivity findings

The connectivity maps generated from each seed-ROI in patients and controls were consistent with previous findings (Di Martino et al., 2008; Lee et al., 2012; Postuma & Dagher, 2006) as shown for basal ganglia, cortical, and cerebellar seeds in Figure S1–S3. Second level comparisons revealed a number of differences between patients and controls, within the patients' group, and between children and adults as detailed in the following paragraphs.

3.2.1 | GLUT1DS versus controls

Group comparisons between GLUT1 and controls demonstrated significant differences in FC in patients when considering all the basal ganglia seeds except the caudate (Table 2). Specifically, GLUT1 patients showed a significant increase in FC between the putamen and globus pallidus and the premotor cortex (respectively medial frontal gyrus and supplementary motor area-SMA). In addition, spontaneous hemodynamic fluctuations in the basal ganglia (putamen and globus pallidus) correlated with the stratum regions, lateralized to the left side (Table 2 and Figure 1). We did not observe significant differences in FC for the ROI placed in the thalamus and caudate nucleus. GLUT1 patients show stronger positive correlations between the cerebellar vermis seeds with the left superior parietal lobule while a decreased FC was detected between the primary visual cortex and the left lingual gyrus (Table 2, Figure 1). No differences in FC were observed when the ROI was placed in the PCU and primary motor cortex.

3.2.2 | Children with GLUT1DS versus healthy children

Table 3 and Figure 2 summarize the FC differences between GLUT1 children and the healthy children. Similarly, to previous comparison,

TABLE 2 Seed-to-voxel functional connectivity differences in all GLUT1 population versus all controls

Seed ROI	Brain region	MNI coordinates (mm)			Z score
		x	*y*	*z*	
Putamen	Medial frontal gyrus-BA11↑	−6	42	−12	4.04
	Putamen L↑	−14	4	6	3.51
Globus pallidus	Supplementary motor area R-BA6↑	16	−10	50	4.20
	Caudate L ↑	−16	22	−6	4.19
Calcarine cortex	Lingual gyrus L-BA17 ↓	−24	−102	−14	4.22
Cerebellar vermis	Superior parietal lobule L-BA7↑	−36	−64	50	4.04

Note: List of the brain regions showing significant (cluster level: $p < .05$ FWE corrected) increase or decrease connectivity with the considered cortical, cerebellar and subcortical ROIs in patients versus controls; ↑: increase functional connectivity; ↓: decrease functional connectivity; BA, Brodmann area; L, left; R, right; Z, Z score of peak of BOLD change.
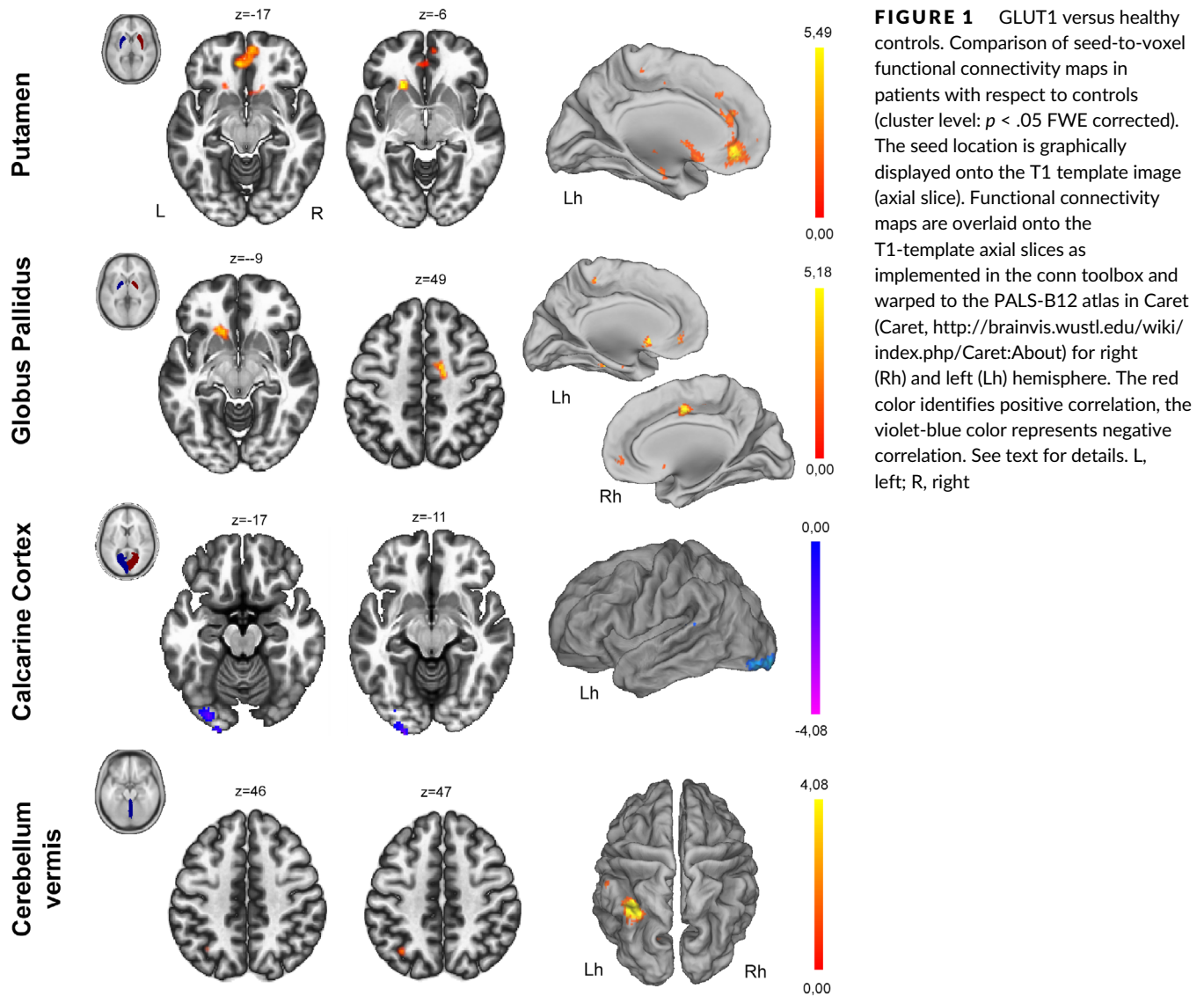
FIGURE 1 GLUT1 versus healthy controls. Comparison of seed-to-voxel functional connectivity maps in patients with respect to controls (cluster level: *p* < .05 FWE corrected). The seed location is graphically displayed onto the T1 template image (axial slice). Functional connectivity maps are overlaid onto the T1-template axial slices as implemented in the conn toolbox and warped to the PALS-B12 atlas in Caret (Caret, http://brainvis.wustl.edu/wiki/index.php/Caret:About) for right (Rh) and left (Lh) hemisphere. The red color identifies positive correlation, the violet-blue color represents negative correlation. See text for details. L, left; R, right

TABLE 3 Seed-to-voxel functional connectivity differences in GLUT1 children versus healthy children

Seed ROI	Brain region	MNI coordinates (mm)			Z score
		x	*y*	*z*	
Putamen	Amygdala R ↑	28	8	−16	4.62
	Medial frontal gyrus L-BA11 ↑	0	52	−26	4.26
	Putamen R ↑	20	8	14	4.23
	Globus pallidus L ↑	−16	−2	4	3.88
Globus pallidus	Putamen R ↑	20	10	16	4.31
	Caudate L ↑	−14	18	−6	4.18
Calcarine cortex	Globus pallidus R ↑	20	−10	2	4.89
Motor cortex	Middle frontal gyrus L-BA6 ↓	−20	−6	46	4.35

Note: List of the brain regions showing significant (cluster level: *p* < .05 FWE corrected) increase or decrease connectivity with the considered cortical and subcortical ROIs in patients children (<18 years) versus healthy children. ↑: increase functional connectivity; ↓: decrease functional connectivity; BA, Brodmann area; L, left; R, right; Z, Z score of peak of BOLD changes.
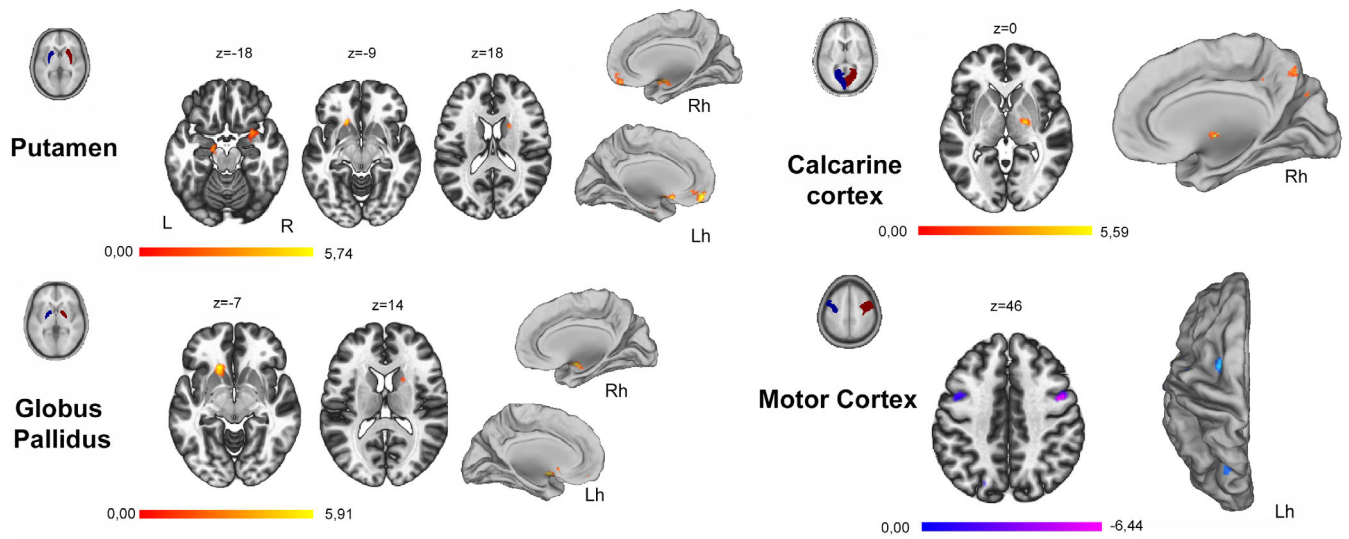
FIGURE 2 GLUT1 children versus healthy children. Comparison of seed-to-voxel functional connectivity maps in patients (children) with respect to controls (children; cluster level: *p* < .05 FWE corrected). The seed location is graphically displayed onto the T1 template image (axial slice). Functional connectivity maps are overlaid onto the T1-template axial slices as implemented in the conn toolbox and warped to the PALS-B12 atlas in Caret (Caret, http://brainvis.wustl.edu/wiki/index.php/Caret:About) for right (Rh) and left (Lh) hemisphere. The red color identifies positive correlation, the violet-blue color represents negative correlation. See text for details. L, left; R, right

TABLE 4 Seed-to-voxel functional connectivity differences in GLUT1 adults versus healthy adults

| Seed ROI | Brain region | MNI coordinates (mm) | | | Z score |
		x	y	z	
Caudate	Cerebellum hemisphere L ↑	−18	−70	−22	4.25
Calcarine cortex	Lingual gyrus L-BA17 ↑	−24	−104	−10	4.57

Note: List of the brain regions showing significant (cluster level: *p* < .05 FWE corrected) connectivity changes with the considered cortical and subcortical ROIs in patients adults (>18 years old) versus controls adults. ↑ : increase functional connectivity; ↓ : decrease functional connectivity; BA, Brodmann area; L, left; R, right; Z, Z score of peak of activation.

FIGURE 3 GLUT1 adults versus healthy adults. Comparison of seed-to-voxel functional connectivity maps in patients (adults) with respect to controls (adults; cluster level: *p* < .05 FWE corrected). The seed location is graphically displayed onto the T1 template image (axial slice). Functional connectivity maps are overlaid onto the T1-template axial slices as implemented in the conn toolbox and warped to the PALS-B12 atlas in Caret (Caret, http://brainvis.wustl.edu/wiki/index.php/Caret:About) for right (Rh) and left (Lh) hemisphere and for cerebellum (PALS Cerebral, Colin Cerebellar). The red color identifies positive correlation, the violet-blue color represents negative correlation. See text for details. L, left; R, right
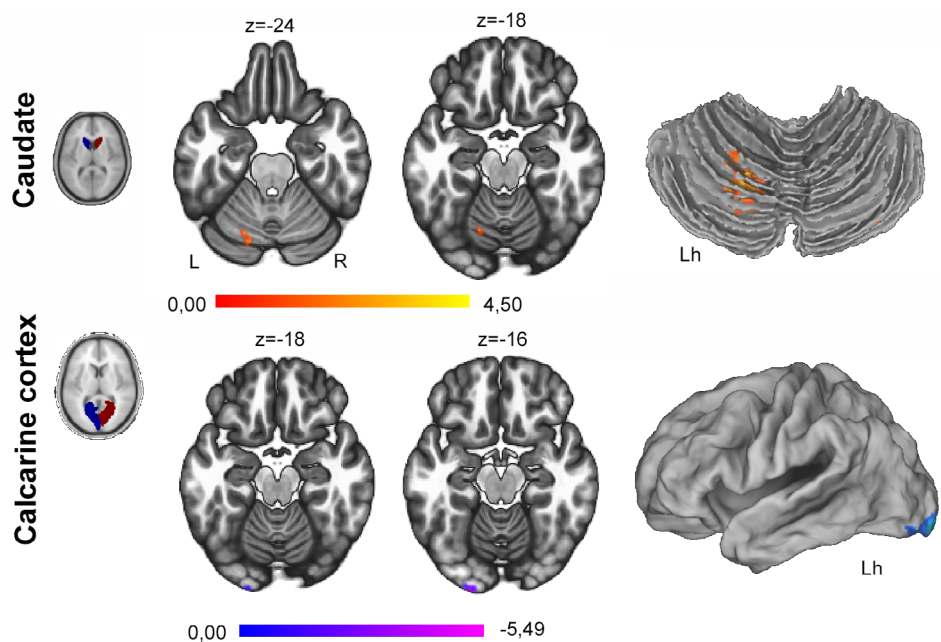
the putamen and globus pallidus seeds demonstrated higher FC with the basal ganglia nuclei of both hemispheres and with the frontal cortex (prefrontal regions) lateralized to the left hemisphere. Intriguingly, the putamen activity correlated with the right amygdala more in patients with respect to controls. When considered the cortical seeds, the children with GLUT1DS shown reduced connectivity within the primary motor cortex and the left premotor areas (middle frontal gyrus). By contrary, calcarine cortex seeds positively correlated more than controls with the globus pallidus (Figure 2).

3.2.3 | Adults with GLUT1DS versus healthy adults

A very few of differences were observed in the seed-to-voxel connectivity comparison analysis between adults with GLUT1 and healthy adults (Table 4 and Figure 3).

TABLE 5 Seed-to-voxel functional connectivity differences in GLUT1 children versus GLUT1 adults

Seed ROI	Brain region	MNI coordinates (mm)			Z score
		x	y	z	
Putamen	Caudate R	16	4	22	3.97
Globus pallidus	Caudate R	16	4	24	4.53

Note: List of the brain regions showing significant (cluster level: *p* < .05 FWE corrected) increase connectivity with the considered cortical, cerebellar, and subcortical ROIs in children GLUT1 versus adults GLUT1. L, left; R, right.
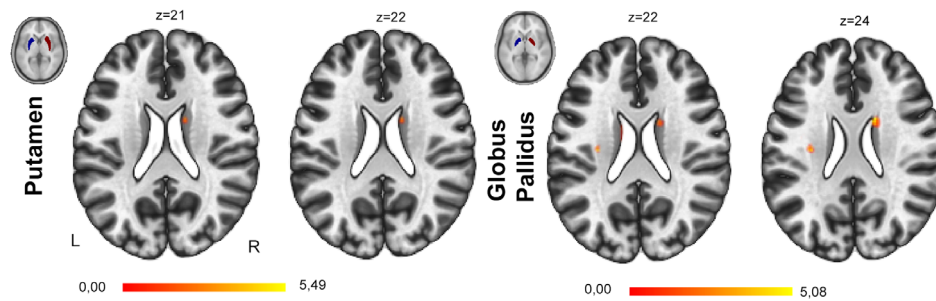
3.2.4 | Children with GLUT1DS versus adults with GLUT1DS

Results are summarized in the Table 5 and Figure 4. Overall, GLUT1 children demonstrated increased correlations within the basal ganglia circuits and specifically between the putamen and the globus pallidus seed with the right caudate nucleus. In controls, no differences in FC between children and adults were detected for the considered seeds (data not shown).

3.2.5 | Correlation between connectivity measures and clinical variables

There were no significant correlations between the seeds connectivity measures and clinical variables: (a) age at diagnosis; (b) seizure's onset age; (c) intelligence quotient-IQ; (d) glycorrhachia; and (e) MD's onset age.

Finally, we evaluated if the presence at diagnosis or at the time of the fMRI study of PED and other MDs affected the connectivity patterns. We found that patients with MD at the time of diagnosis demonstrated higher FC between basal ganglia seeds (putamen and globus pallidus) and the cerebellum (left posterior lobe; Table 6 and Figure 5, Panel A) compared to patients without MDs. On parallel, cerebellar hemisphere seeds correlates with the caudate nucleus in GLUT1DS with MD more than in GLUT1DS without MD (Figure 5, Panel B). This abnormal connectivity pattern was confirmed in those GLUT1DS with MDs at the time of fMRI study when compared with patients without MD during the disease course.

FIGURE 4 GLUT1 children versus GLUT1 adults. Comparison of seed-to-voxel functional connectivity maps in patients' children with respect to patients' adults (cluster level: *p* < .05 FWE corrected). The seed location is graphically displayed onto the T1 template image (axial slice). Functional connectivity maps are overlaid onto the T1-template axial slices as implemented in the conn toolbox. The red color identifies positive correlation. See text for details. L, left; R, right

TABLE 6 Seed-to-voxel functional connectivity differences in GLUT1 with MD versus GLUT1 without MD

Seed ROI	Brain region	MNI coordinates (mm)			Z score
		x	y	z	
Putamen	Cerebellum L-posterior lobe	−8	−90	−24	5.33
Globus pallidus	Cerebellum L-posterior lobe	−8	−88	−24	4.74
Cerebellar hemisphere	Caudate head R	16	22	−4	4.03

Note: List of the brain regions showing significant (cluster level: *p* < .05 FWE corrected) increase connectivity with the considered cortical and subcortical ROIs in GLUT1 with MD versus GLUT1 without MD at the time of diagnosis. L, left; R, right.
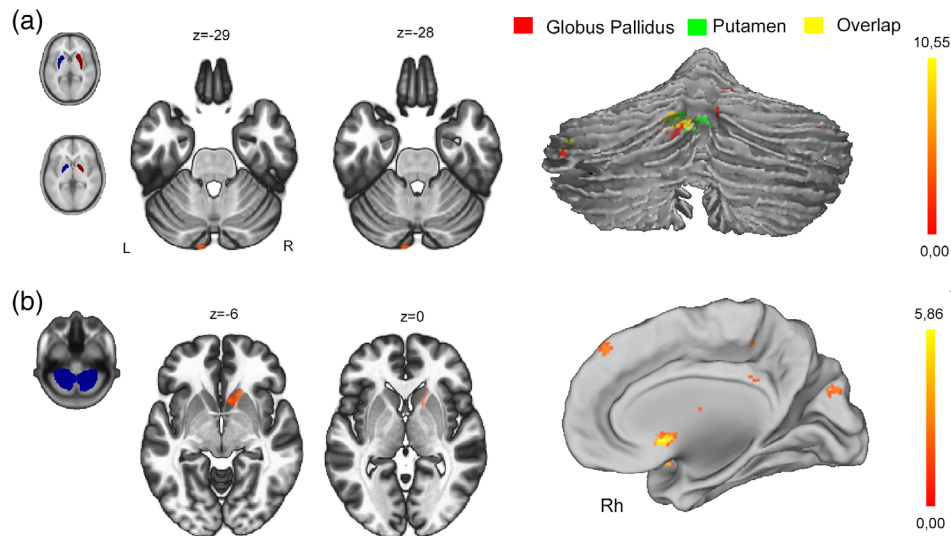
FIGURE 5 GLUT1DS with MD versus GLUT1DS without MD. Panel A: Comparison of putamen and globus pallidus seeds functional connectivity maps in patients with MD (at the time of diagnosis) respect to patients without MD (cluster level: $p < .05$ FWE corrected). The subcortical seed location is graphically displayed onto the T1 template image (axial slice). Functional connectivity maps are overlaid onto the T1-template axial slices as implemented in the conn toolbox and warped to the atlas in Caret (Caret, http://brainvis.wustl.edu/wiki/index.php/Caret:About) for cerebellum (PALS Cerebral, Colin Cerebellar). Panel B: Comparison of cerebellar hemisphere seeds functional connectivity maps in patients with MD (at the time of diagnosis) respect to patients without MD (cluster level: $p < .05$ FWE corrected). The cerebellar seeds' location is graphically displayed onto the T1 template image (axial slice). Functional connectivity maps are overlaid onto the T1-template axial slices as implemented in the conn toolbox and warped to the PALS-B12 atlas in Caret (Caret, http://brainvis.wustl.edu/wiki/index.php/Caret:About) for the right (Rh) hemisphere (mesial view). See text for details. L, left; R, right

4 | DISCUSSION

This is the first study to examine the brain state FC at rest in patients with GLUT1DS compared to healthy controls. As main finding, converging evidence indicated in GLUT1DS, an hyper-connectivity in cortical and subcortical brain networks involved in motor planning, control and learning represented by the premotor cortex, basal ganglia circuits (especially striatum) and cerebellum. Interestingly, the increase in connectivity was predominant in those patients with PED and MDs (at the time of diagnosis), and in children with respect to adults, thus suggesting a correlation with the clinical phenotype. This neuroimaging picture is in line with previous PET findings in GLUT1 patients (Pascual et al., 2007; Pascual, Van Heertum, Wang, Engelstad, & De Vivo, 2002; Suls et al., 2008). It thus emerges a highly reproducible functional radiological signature of the disease that allow the recognition of key nodes (basal ganglia, motor, and premotor cortex), potentially target of new therapeutic approaches. Very recently, the long-term effect of globus pallidus internus (GPi) deep brain stimulation in GLUT1DS has been reported, even limited to a single case (Hanci et al., 2018).

4.1 | Segregated pattern of striatal involvement in GLUT1DS

Overall considered, the present findings show a dysfunction of striatum's circuitries in GLUT1DS at rest. The putamen has been already identified as central hub for the occurrence of PED in GLUT1 patients. Both interictal PET (Pascual et al., 2007; Pascual, Van

Heertum, Wang, Engelstad, & De Vivo, 2002) and ictal SPECT during a PED episode (Suls et al., 2008) demonstrated an increase metabolic and perfusional pattern of this deep structure. Herein, we move forward and we show an hyper-activity of both globes pallidus and putamen, while the caudate nucleus resulted less involved. Interestingly, FC analyses shown a local hyper-connectivity within the striatum circuits, generating a sort of self-reinforcing circuit. This effect was observed when comparing the patients versus controls (Figure 1) and especially GLUT1 children versus adults (Figure 4). Several mechanisms may account for this increased local intrinsic connectivity. It might reflect an aberrant over-excitability of these structures that in turn led to a sustained disinhibition of the cortical and cerebellar regions implicated in the motor planning, execution, and control. Additionally, the within-striatum increased FC may be a sign of functional re-organization of the brain in response to chronic reduced glucose uptake. Such reorganization theoretically occurs by means of increased activation and/or synchronization of specific brain regions or networks (Saggar et al., 2017; Schoonheim, Geurts, & Barkhof, 2010). Sustained neuroglycopenia, as observed in GLUT1DS, might reinforce FC via neuroplasticity-related mechanisms, representing an adaptive brain response. Children with diabetes and, similarly, adults with diabetes exposed to experimental hypoglycemia showed increased in connectivity across different RSN and brain nodes including the basal ganglia circuits (Bolo et al., 2015; Saggar et al., 2017). Interestingly, the functional reorganization and resulting changes in FC may represent an early and finite phenomenon, as the compensatory changes can be lost with disease progression (Roosendaal et al.,

2010). To note, the abnormal hyper-synchronization within the striatum regions is attenuated in adulthood. Both putamen and globus pallidus appeared hyperconnected with the frontal cortex in GLUT1DS patients more than controls. This pattern is particularly evident in the affected children subpopulation. The globus pallidus seeds predicted activity in premotor regions (i.e., supplementary motor area) consistently with its known involvement in movement (Postuma & Dagher, 2006; Saga, Hoshi, & Tremblay, 2017). Putamen seeds positively correlate with associative frontal regions implicated in executive function control reproducing the FC of the rostral putamen division observed in controls (Di Martino et al., 2008). Executive functions and attention impairment have been reported in GLUT1DS (De Giorgis et al., 2019; Ragona et al., 2014).

4.2 | Correlation between FC maps and the clinical phenotype: The effect of MD presence

We examined differences in between seed-based network connectivity in patients with PED at the time of diagnosis (and at fMRI scan) versus patients without. Our findings demonstrated an increase in the connectivity between the lenticular nucleus with the posterior lobe of the cerebellum in those patients with PED, both at onset and during follow-up (Figure 5). Intriguingly, a specular connectivity pattern was demonstrated when the seed was located in the cerebellar hemispheres (Table 6). We hypothesized that such "cerebellar-striatum" hyper-connectivity is the intrinsic functional substrate of PED appearance. In this line, patients with paroxysmal kinesigenic dyskinesia (PKD) shown abnormal increased homotopic resting state FC between the two cerebellar hemispheres together with hyper-connectivity of the basal ganglia circuits (Ren et al., 2015). Similarly, SPECT imaging shown hyperperfusion of cerebellum during the motor attacks (Kluge et al., 1998). The limited number of GLUT1DS patients with and without MD in each group limited the generalizability of our findings and need to be validated in larger cohort of patients with similar clinical presentation.

4.3 | Correlation between FC maps and the clinical phenotype: The effect of age

The cohort of GLUT1 patients investigated includes children and adults allowing to infer about differences in functional brain networks architecture at different ages. As main finding, we observed abnormal connectivity patterns of many cortical–subcortical hubs in children when compared to controls, while in adults these differences were attenuated. Similarly, a direct comparison between GLUT1 children versus adults demonstrated, only in the former, an increased in the connectivity between the striatal seeds (Figure 4). These results support previous observations of negative correlation between interhemispheric putamen connectivity at rest and illness duration in patients with PKD (Ren et al., 2015). It is likely that the excessive increase in FC as revealed by our analyses tends to decrease to normal level with the prolongation of the disease, implying that some compensation mechanisms could be developed. This might reflect the clinical course of the GLUT1 encephalopathy that tends spontaneously to compensate over time or, alternatively,

it could be a positive long-term effect linked to the long course medical and dietary treatment (Shiohama, Fujii, Takahashi, Nakamura, & Kohno, 2013). Overall, our results reinforce previous clinical observations of the age-dependency of clinical manifestations (Alter et al., 2015; De Giorgis & Veggiotti, 2013; Pearson et al., 2017) and not-progressive evolution of this encephalopathy (Akman et al., 2015). To note, previous single-case structural MR study in GLUT1 demonstrated the reversibility of T2 WM lesion during follow-up (Shiohama, Fujii, Takahashi, Nakamura, & Kohno, 2013).

4.4 | Chronic neuroglycopenia and FC

Resting state activity reflects metabolic processes as revealed by simultaneous FDG-PET/fMRI studies (Nugent, Martinez, D'Alfonso, Zarate, & Theodore, 2015; Riedl et al., 2014; Tomasi, Wang, & Volkow, 2013). Increases in local neuronal activity and hence in glucose metabolism coincide almost exactly with the spatial pattern of increase in resting state FC (Riedl et al., 2014). Emerging evidences indicate that brain regions may differ in metabolic activity and metabolic supply associations based on regional morphometric and functional proprieties. Under physiological conditions, during rest, the relationship between the glucose utilization and neuroglial activity is heterogeneously distributed with brain regions showing concurrent higher energy utilization and activity (like medial visual and default mode network) and others demonstrating a deviation between glucose utilization and neuroglial activity (Shokri-Kojori et al., 2019). The use of energy source other than glucose such as keton bodies could contribute to explain such discrepancy. Patients with GLUT1DS are exposed to chronic neuroglycopenia due to the impaired glucose transport across the blood–brain barrier (Akman et al., 2010; De Vivo & Wang, 2008). Low GLUT1 protein availability causes delayed brain angiogenesis and microvascular diminution (Tang et al., 2017). The direct consequence of transport insufficiency and altered vascular architecture is a reduced energy supply to astrocytes and then to neurons, interfering with the neurotransmission at rest and especially under situations of extra metabolic demand (Pascual, Van Heertum, Wang, Engelstad, & De Vivo, 2002). Our findings of a cortico-subcortical (basal ganglia) hyper-connectivity appears puzzling at first as it would suggest a regional augmented metabolism and local neuronal activity. This behavior is particularly evident within the striatal nuclei circuits and their cortical and cerebellar projections. The striatum is very vulnerable to energy failure, both in hypoglycemia (Auer, Wieloch, Olsson, & Siesjö, 1984; Wieloch, 1985), and in transient reversible ischemia (DeGirolami, Crowell, & Marcoux, 1984). Nevertheless, biochemical studies in primary culture of rat striatal neurons exposed to acute hypoglycemia have shown the existence of a neuroprotective mechanism that allows cells not to die but survive in a form of suspended animation, with sufficient energy to maintain membrane potentials (McDermott, Bradley, McCarron, Palmer, & Morris, 2003). In patients with diabetes, induced hypoglycemia determines broad perturbations of resting state FC patterns with increase connectivity in core nodes including the hypothalamus, basal ganglia, insula, default mode network, sensorimotor, cingulate cortices, and cerebellum while

opposite behavior was detected in nondiabetic controls (Bolo et al., 2015). Interestingly, recurrent hypoglycemia as observed in heavy drinker patients is associated with a stronger positive association between the glucose utilization (measured by FDG-PET) and neuronal-glia activity (expressed local FC) in specific brain regions like cerebellum and precuneus (Shokri-Kojori et al., 2019). Alcohol abuse leads to increase of the brain acetate utilization and the blood–brain-barrier transport of acetate (Jiang et al., 2013). Augmented acetate consumption represents an alternative energy pathway to support brain astroglia metabolism, leaving more glucose available to supply neurons. The cerebellum shows the highest level of acetate metabolism when acetate levels in the plasma are increased thus supporting our findings of its higher FC in GLUT1DS patients more than controls. On the contrary, the primary visual cortex appeared less self-connected in GLUT1DS. The discrepancy between the visual and cerebellum functional behaviors during chronic reduced glucose supply has been documented by FDG-PET and fMRI studies in heavy drinkers (Shokri-Kojori et al., 2019). Different mechanisms of adaptation based on changes in active glucose metabolic pathways (aerobic glycolysis versus oxidative metabolism in the visual cortex) or the use of alternative source of energy (in the cerebellum) might explain this mismatch (Shokri-Kojori, Tomasi, Wiers, Wang, & Volkow, 2017; Volkow et al., 2015). In our patients, the exposure to chronic brain low glucose levels likely modifies energetic and neurotransmitter metabolic pathways by metabolic adaptive mechanisms (Öz et al., 2012; Terpstra et al., 2014; van de Ven, Tack, Heerschap, van der Graaf, & de Galan, 2013), which could underlie the increased connectivity changes in those regions highly sensible to glycopenia. The utilization of alternative source of energy in GLUT1DS to maintain brain activity is of relevance being the rationale behind the use to the KD as the treatment of choice in this complex genetic disorder (Alter et al., 2015; De Giorgis & Veggiotti, 2013).

4.5 | Study limitations

We are aware about some limitations of our study. First, we analyzed the data of a relatively low number of subjects. The subdivision of children and adults in the patients' cohort makes the groups even smaller. However, this is justified by the rarity of this genetic disorder. In addition, as already stated, the clinical manifestations of the syndrome as epilepsy and motor signs were not homogeneously distributed across patients as well as treatment and age at the time of the EEG-fMRI study. This heterogeneous presentation reflects the intrinsic and natural variability of the syndrome, as largely documented (De Giorgis & Veggiotti, 2013; Pearson, Akman, Hinton, Engelstad, & De Vivo, 2013). Noteworthy, as far as we know, this study is unique in term of number of patients investigated as well as the methodology applied. Within the "big data" epoch, further effort must be taken to collect and share MRI data (structural and functional) of rare neurological disorders around world in order to replicate and support the neuroimaging findings based on small series. Second, we limited our analyses to a seed-based FC approach. This approach was chosen based on a strong a priori hypothesis. In this contest, seed-based analysis is the simplest and more appropriate method to explore our hypothesis and improve the scientific understanding (Iraji et al., 2016; Keilholz, Magnuson, & Thompson, 2010). More exploratory data-driven methods can be applied to explore the intrinsic functional networks and how they interact without a priori model of brain activity. In particular, given the reported local hyper-connectivity within the striatum areas, regional homogeneity (ReHo) methods might be applied to explore the local temporal synchrony within the basal ganglia regions providing an estimation of the efficiency of coordinated neuronal activity. Third, almost all patients were on AED treatment during scanning (13/18), which may be a confounding factor influencing the intrinsic brain function, also difference between on and off treatment could not be detected. Similarly, the effect of KD on the resting state fluctuation could not be explored given the limited number of patients on KD without AED at fMRI. Finally, in this study we did not explore microstructural gray matter abnormalities neither the volume of subcortical nuclei in GLUT1DS. So, the influence of structural abnormalities to resting state FC cannot be excluded. However, at visual expert evaluation, no defects in gray and WM were observed in any patients/controls.

4.6 | Conclusions

We demonstrated an increase in connectivity at rest mainly in the basal ganglia-frontal-cerebellum circuitry. We highlighted the primary role of the striatum in the pathophysiology of this encephalopathy. The revealed dysfunctional connectivity pattern is not stable across the lifespan but move toward normality in adulthood, in agreement with the clinical scenario. GLUT1DS can be a model to explore the effect of neuroglycopenia on the brain function. In this contest, our results may portrait the effect of neuroprotective brain strategy to overcome the chronic poor energy supply during vulnerable ages.

DATA AVAILABILITY STATEMENT

The data that support the findings of this study are available from the corresponding author upon reasonable request.

ORCID

Anna Elisabetta Vaudano https://orcid.org/0000-0002-6280-7526

REFERENCES

Akman, C. I., Engelstad, K., Hinton, V. J., Ullner, P., Koenigsberger, D., Leary, L., ... De Vivo, D. C. (2010). Acute hyperglycemia produces transient improvement in glucose transporter type 1 deficiency. *Annals of Neurology*, 67(1), 31–40. https://doi.org/10.1002/ana.21797

Akman, C. I., Provenzano, F., Wang, D., Engelstad, K., Hinton, V., Yu, J., ... De Vivo, D. C. (2015). Topography of brain glucose hypometabolism and epileptic network in glucose transporter 1 deficiency. *Epilepsy Research*, 110, 206–215. https://doi.org/10.1016/j.eplepsyres.2014.11.007

Allen, P. J., Josephs, O., & Turner, R. (2000). A method for removing imaging artifact from continuous EEG recorded during functional MRI. *NeuroImage*, 12(2), 230–239. https://doi.org/10.1006/nimg.2000.0599

Allen, P. J., Polizzi, G., Krakow, K., Fish, D. R., & Lemieux, L. (1998). Identification of EEG events in the MR scanner: The problem of pulse artifact and a method for its subtraction. *NeuroImage*, 8(3), 229–239. https://doi.org/10.1006/nimg.1998.0361

Alter, A. S., Engelstad, K., Hinton, V. J., Montes, J., Pearson, T. S., Akman, C. I., & De Vivo, D. C. (2015). Long-term clinical course of Glut1 deficiency syndrome. *Journal of Child Neurology*, 30(2), 160–169. https://doi.org/10.1177/0883073814531822

Arsov, T., Mullen, S. A., Rogers, S., Phillips, A. M., Lawrence, K. M., Damiano, J. A., ... Scheffer, I. E. (2012). Glucose transporter 1 deficiency in the idiopathic generalized epilepsies. *Annals of Neurology*, 72(5), 807–815. https://doi.org/10.1002/ana.23702

Attwell, D., & Laughlin, S. B. (2001). An energy budget for signaling in the grey matter of the brain. *Journal of Cerebral Blood Flow and Metabolism: Official Journal of the International Society of Cerebral Blood Flow and Metabolism*, 21(10), 1133–1145. https://doi.org/10.1097/00004647-200110000-00001

Auer, R. N., Wieloch, T., Olsson, Y., & Siesjö, B. K. (1984). The distribution of hypoglycemic brain damage. *Acta Neuropathologica*, 64(3), 177–191.

Avanzini, P., Vaudano, A. E., Vignoli, A., Ruggieri, A., Benuzzi, F., Darra, F., ... Meletti, S. (2014). Low frequency mu-like activity characterizes cortical rhythms in epilepsy due to ring chromosome 20. *Clinical Neurophysiology: Official Journal of the International Federation of Clinical Neurophysiology*, 125(2), 239–249. https://doi.org/10.1016/j.clinph.2013.07.009

Azeez, A. K., & Biswal, B. B. (2017). A review of resting-state analysis methods. *Neuroimaging Clinics of North America*, 27(4), 581–592. https://doi.org/10.1016/j.nic.2017.06.001

Behzadi, Y., Restom, K., Liau, J., & Liu, T. T. (2007). A component based noise correction method (CompCor) for BOLD and perfusion based fMRI. *NeuroImage*, 37(1), 90–101. https://doi.org/10.1016/j.neuroimage.2007.04.042

Bell, A. J., & Sejnowski, T. J. (1995). An information-maximization approach to blind separation and blind deconvolution. *Neural Computation*, 7(6), 1129–1159.

Bertoli, S., Trentani, C., Ferraris, C., De Giorgis, V., Veggiotti, P., & Tagliabue, A. (2014). Long-term effects of a ketogenic diet on body composition and bone mineralization in GLUT-1 deficiency syndrome: A case series. *Nutrition (Burbank, Los Angeles County, CAL)*, 30(6), 726–728. https://doi.org/10.1016/j.nut.2014.01.005

Bolo, N. R., Musen, G., Simonson, D. C., Nickerson, L. D., Flores, V. L., Siracusa, T., ... Jacobson, A. M. (2015). Functional connectivity of insula, basal ganglia, and prefrontal executive control networks during hypoglycemia in type 1 diabetes. *The Journal of Neuroscience: The Official Journal of the Society for Neuroscience*, 35(31), 11012–11023. https://doi.org/10.1523/JNEUROSCI.0319-15.2015

Brockmann, K., Wang, D., Korenke, C. G., von Moers, A., Ho, Y. Y., Pascual, J. M., ... De Vivo, D. C. (2001). Autosomal dominant glut-1 deficiency syndrome and familial epilepsy. *Annals of Neurology*, 50(4), 476–485.

Cao, X., Cao, Q., Long, X., Sun, L., Sui, M., Zhu, C., ... Wang, Y. (2009). Abnormal resting-state functional connectivity patterns of the putamen in medication-naïve children with attention deficit hyperactivity disorder. *Brain Research*, 1303, 195–206. https://doi.org/10.1016/j.brainres.2009.08.029

Chai, X. J., Castañón, A. N., Ongür, D., & Whitfield-Gabrieli, S. (2012). Anticorrelations in resting state networks without global signal regression. *NeuroImage*, 59(2), 1420–1428. https://doi.org/10.1016/j.neuroimage.2011.08.048

Ciric, R., Wolf, D. H., Power, J. D., Roalf, D. R., Baum, G. L., Ruparel, K., ... Satterthwaite, T. D. (2017). Benchmarking of participant-level confound regression strategies for the control of motion artifact in studies of functional connectivity. *NeuroImage*, 154, 174–187. https://doi.org/10.1016/j.neuroimage.2017.03.020

De Giorgis, V., Masnada, S., Varesio, C., Chiappedi, M. A., Zanaboni, M., Pasca, L., ... Veggiotti, P. (2019). Overall cognitive profiles in patients with GLUT1 deficiency syndrome. *Brain and Behavior*, 9(3), e01224. https://doi.org/10.1002/brb3.1224

De Giorgis, V., Teutonico, F., Cereda, C., Balottin, U., Bianchi, M., Giordano, L., ... Veggiotti, P. (2015). Sporadic and familial glut1ds Italian patients: A wide clinical variability. *Seizure*, 24, 28–32. https://doi.org/10.1016/j.seizure.2014.11.009

De Giorgis, V., & Veggiotti, P. (2013). GLUT1 deficiency syndrome 2013: Current state of the art. *Seizure*, 22(10), 803–811. https://doi.org/10.1016/j.seizure.2013.07.003

De Vivo, D. C., Trifiletti, R. R., Jacobson, R. I., Ronen, G. M., Behmand, R. A., & Harik, S. I. (1991). *Defective glucose transport across the blood-brain barrier as a cause of persistent hypoglycorrhachia, seizures, and developmental delay*. Retrieved from https://www.ncbi.nlm.nih.gov/pubmed/1714544

De Vivo, D. C., & Wang, D. (2008). Glut1 deficiency: CSF glucose. How low is too low? *Revue Neurologique*, 164(11), 877–880. https://doi.org/10.1016/j.neurol.2008.10.001

DeGirolami, U., Crowell, R. M., & Marcoux, F. W. (1984). Selective necrosis and total necrosis in focal cerebral ischemia. Neuropathologic observations on experimental middle cerebral artery occlusion in the macaque monkey. *Journal of Neuropathology and Experimental Neurology*, 43(1), 57–71. https://doi.org/10.1097/00005072-198401000-00005

Di Martino, A., Scheres, A., Margulies, D. S., Kelly, A. M. C., Uddin, L. Q., Shehzad, Z., ... Milham, M. P. (2008). Functional connectivity of human striatum: A resting state FMRI study. *Cerebral Cortex (New York, N.Y.: 1991)*, 18(12), 2735–2747. https://doi.org/10.1093/cercor/bhn041

Fonov, V., Evans, A. C., Botteron, K., Almli, C. R., McKinstry, R. C., Collins, D. L., & Brain Development Cooperative Group. (2011). Unbiased average age-appropriate atlases for pediatric studies. *NeuroImage*, 54(1), 313–327. https://doi.org/10.1016/j.neuroimage.2010.07.033

Hanci, I., Kamm, C., Scholten, M., Roncoroni, L. P., Weber, Y., Krüger, R., ... Weiss, D. (2018). Long-term effect of GPi-DBS in a patient with generalized dystonia due to GLUT1 deficiency syndrome. *Frontiers in Neurology*, 9, 381. https://doi.org/10.3389/fneur.2018.00381

Hully, M., Vuillaumier-Barrot, S., Le Bizec, C., Boddaert, N., Kaminska, A., Lascelles, K., ... Bahi-Buisson, N. (2015). From splitting GLUT1 deficiency syndromes to overlapping phenotypes. *European Journal of*

Medical Genetics, 58(9), 443–454. https://doi.org/10.1016/j.ejmg.2015.06.007

Iraji, A., Calhoun, V. D., Wiseman, N. M., Davoodi-Bojd, E., Avanaki, M. R. N., Haacke, E. M., & Kou, Z. (2016). The connectivity domain: Analyzing resting state fMRI data using feature-based data-driven and model-based methods. NeuroImage, 134, 494–507. https://doi.org/10.1016/j.neuroimage.2016.04.006

Ishibashi, K., Sakurai, K., Shimoji, K., Tokumaru, A. M., & Ishii, K. (2018). Altered functional connectivity of the default mode network by glucose loading in young healthy participants. BMC Neuroscience, 19(1), 33. https://doi.org/10.1186/s12868-018-0433-0

Jiang, L., Gulanski, B. I., De Feyter, H. M., Weinzimer, S. A., Pittman, B., Guidone, E., … Mason, G. F. (2013). Increased brain uptake and oxidation of acetate in heavy drinkers. The Journal of Clinical Investigation, 123(4), 1605–1614. https://doi.org/10.1172/JCI65153

Keilholz, S. D., Magnuson, M., & Thompson, G. (2010). Evaluation of data-driven network analysis approaches for functional connectivity MRI. Brain Structure & Function, 215(2), 129–140. https://doi.org/10.1007/s00429-010-0276-7

Di Martino, A., Kelly, C., Grzadzinski, R., Zuo, X.-N., Mennes, M., Mairena, M. A., … Milham, M. P. (2011). Aberrant striatal functional connectivity in children with autism. Biological Psychiatry, 69(9), 847–856. https://doi.org/10.1016/j.biopsych.2010.10.029

Klepper, J. (2012). GLUT1 deficiency syndrome in clinical practice. Epilepsy Research, 100(3), 272–277. https://doi.org/10.1016/j.eplepsyres.2011.02.007

Klepper, J. (2008). Glucose transporter deficiency syndrome (GLUT1DS) and the ketogenic diet. Epilepsia, 49(Suppl. 8), 46–49. https://doi.org/10.1111/j.1528-1167.2008.01833.x

Klepper, J., Engelbrecht, V., Scheffer, H., van der Knaap, M. S., & Fiedler, A. (2007). GLUT1 deficiency with delayed myelination responding to ketogenic diet. Pediatric Neurology, 37(2), 130–133. https://doi.org/10.1016/j.pediatrneurol.2007.03.009

Kluge, A., Kettner, B., Zschenderlein, R., Sandrock, D., Munz, D. L., Hesse, S., & Meierkord, H. (1998). Changes in perfusion pattern using ECD-SPECT indicate frontal lobe and cerebellar involvement in exercise-induced paroxysmal dystonia. Movement Disorders: Official Journal of the Movement Disorder Society, 13(1), 125–134. https://doi.org/10.1002/mds.870130124

Lee, M. H., Smyser, C. D., & Shimony, J. S. (2013). Resting-state fMRI: A review of methods and clinical applications. AJNR. American Journal of Neuroradiology, 34(10), 1866–1872. https://doi.org/10.3174/ajnr.A3263

Lee, M. H., Smyser, C. D., & Shimony, J. S. (2013). Resting-state fMRI: A review of methods and clinical applications. AJNR. American Journal of Neuroradiology, 34(10), 1866–1872. https://doi.org/10.3174/ajnr.A3263 Leen, W. G., Taher, M., Verbeek, M. M., Kamsteeg, E. J., van de Warrenburg, B. P., & Willemsen, M. A. (2014). GLUT1 deficiency syndrome into adulthood: A follow-up study. Journal of Neurology, 261(3), 589–599. https://doi.org/10.1007/s00415-014-7240-z

Leen, W. G., Wevers, R. A., Kamsteeg, E.-J., Scheffer, H., Verbeek, M. M., & Willemsen, M. A. (2013). Cerebrospinal fluid analysis in the workup of GLUT1 deficiency syndrome: A systematic review. JAMA Neurology, 70(11), 1440–1444. https://doi.org/10.1001/jamaneurol.2013.3090

Logothetis, N. K., Pauls, J., Augath, M., Trinath, T., & Oeltermann, A. (2001). Neurophysiological investigation of the basis of the fMRI signal. Nature, 412(6843), 150–157. https://doi.org/10.1038/35084005

Makeig, S., Debener, S., Onton, J., & Delorme, A. (2004). Mining event-related brain dynamics. Trends in Cognitive Sciences, 8(5), 204–210. https://doi.org/10.1016/j.tics.2004.03.008

McDermott, C. J., Bradley, K. N., McCarron, J. G., Palmer, A. M., & Morris, B. J. (2003). Striatal neurones show sustained recovery from severe hypoglycaemic insult. Journal of Neurochemistry, 86(2), 383–393.

Nugent, A. C., Martinez, A., D'Alfonso, A., Zarate, C. A., & Theodore, W. H. (2015). The relationship between glucose metabolism, resting-state fMRI BOLD signal, and GABAA-binding potential: A preliminary study in healthy subjects and those with temporal lobe epilepsy. Journal of Cerebral Blood Flow and Metabolism: Official Journal of the International Society of Cerebral Blood Flow and Metabolism, 35(4), 583–591. https://doi.org/10.1038/jcbfm.2014.228

Öz, G., Tesfaye, N., Kumar, A., Deelchand, D. K., Eberly, L. E., & Seaquist, E. R. (2012). Brain glycogen content and metabolism in subjects with type 1 diabetes and hypoglycemia unawareness. Journal of Cerebral Blood Flow and Metabolism: Official Journal of the International Society of Cerebral Blood Flow and Metabolism, 32(2), 256–263. https://doi.org/10.1038/jcbfm.2011.138

Pascual, J. M., Van Heertum, R. L., Wang, D., Engelstad, K., & De Vivo, D. C. (2002). Imaging the metabolic footprint of Glut1 deficiency on the brain. Annals of Neurology, 52(4), 458–464. https://doi.org/10.1002/ana.10311

Pascual, J. M., Wang, D., Hinton, V., Engelstad, K., Saxena, C. M., Van Heertum, R. L., & De Vivo, D. C. (2007). Brain glucose supply and the syndrome of infantile neuroglycopenia. Archives of Neurology, 64(4), 507–513. https://doi.org/10.1001/archneur.64.4.noc60165

Pearson, T. S., Akman, C., Hinton, V. J., Engelstad, K., & De Vivo, D. C. (2013). Phenotypic spectrum of glucose transporter type 1 deficiency syndrome (Glut1 DS). Current Neurology and Neuroscience Reports, 13(4), 342. https://doi.org/10.1007/s11910-013-0342-7

Pearson, T. S., Pons, R., Engelstad, K., Kane, S. A., Goldberg, M. E., & De Vivo, D. C. (2017). Paroxysmal eye-head movements in Glut1 deficiency syndrome. Neurology, 88(17), 1666–1673. https://doi.org/10.1212/WNL.0000000000003867

Postuma, R. B., & Dagher, A. (2006). Basal ganglia functional connectivity based on a meta-analysis of 126 positron emission tomography and functional magnetic resonance imaging publications. Cerebral Cortex (New York, N.Y.: 1991), 16(10), 1508–1521. https://doi.org/10.1093/cercor/bhj088

Ragona, F., Matricardi, S., Castellotti, B., Patrini, M., Freri, E., Binelli, S., & Granata, T. (2014). Refractory absence epilepsy and glut1 deficiency syndrome: A new case report and literature review. Neuropediatrics, 45(5), 328–332. https://doi.org/10.1055/s-0034-1378130

Ramm-Pettersen, A., Nakken, K. O., Skogseid, I. M., Randby, H., Skei, E. B., Bindoff, L. A., & Selmer, K. K. (2013). Good outcome in patients with early dietary treatment of GLUT-1 deficiency syndrome: Results from a retrospective Norwegian study. Developmental Medicine and Child Neurology, 55(5), 440–447. https://doi.org/10.1111/dmcn.12096

Ren, J., Lei, D., Yang, T., An, D., Xiao, F., Li, L., … Zhou, D. (2015). Increased interhemispheric resting-state functional connectivity in paroxysmal kinesigenic dyskinesia: A resting-state fMRI study. Journal of the Neurological Sciences, 351(1–2), 93–98. https://doi.org/10.1016/j.jns.2015.02.046

Riedl, V., Bienkowska, K., Strobel, C., Tahmasian, M., Grimmer, T., Förster, S., … Drzezga, A. (2014). Local activity determines functional connectivity in the resting human brain: A simultaneous FDG-PET/fMRI study. The Journal of Neuroscience: The Official Journal of the Society for Neuroscience, 34(18), 6260–6266. https://doi.org/10.1523/JNEUROSCI.0492-14.2014

Roosendaal, S. D., Schoonheim, M. M., Hulst, H. E., Sanz-Arigita, E. J., Smith, S. M., Geurts, J. J. G., & Barkhof, F. (2010). Resting state networks change in clinically isolated syndrome. Brain: A Journal of Neurology, 133(Pt 6), 1612–1621. https://doi.org/10.1093/brain/awq058

Roulet-Perez, E., Ballhausen, D., Bonafé, L., Cronel-Ohayon, S., & Maeder-Ingvar, M. (2008). Glut-1 deficiency syndrome masquerading as idiopathic generalized epilepsy. Epilepsia, 49(11), 1955–1958. https://doi.org/10.1111/j.1528-1167.2008.01654.x

Saga, Y., Hoshi, E., & Tremblay, L. (2017). Roles of multiple Globus pallidus territories of monkeys and humans in motivation, cognition and action:

An anatomical, physiological and pathophysiological review. *Frontiers in Neuroanatomy*, *11*, 30. https://doi.org/10.3389/fnana.2017.00030

Saggar, M., Tsalikian, E., Mauras, N., Mazaika, P., White, N. H., Weinzimer, S., ... Reiss, A. L. (2017). Compensatory hyperconnectivity in developing brains of young children with type 1 diabetes. *Diabetes*, *66*(3), 754–762. https://doi.org/10.2337/db16-0414

Savio, A., Fünger, S., Tahmasian, M., Rachakonda, S., Manoliu, A., Sorg, C., ... Yakushev, I. (2017). Resting-state networks as simultaneously measured with functional MRI and PET. *Journal of Nuclear Medicine: Official Publication, Society of Nuclear Medicine*, *58*(8), 1314–1317. https://doi.org/10.2967/jnumed.116.185835

Schoonheim, M. M., Geurts, J. J. G., & Barkhof, F. (2010). The limits of functional reorganization in multiple sclerosis. *Neurology*, *74*(16), 1246–1247. https://doi.org/10.1212/WNL.0b013e3181db9957

Shiohama, T., Fujii, K., Takahashi, S., Nakamura, F., & Kohno, Y. (2013). Reversible white matter lesions during ketogenic diet therapy in glucose transporter 1 deficiency syndrome. *Pediatric Neurology*, *49*(6), 493–496. https://doi.org/10.1016/j.pediatrneurol.2013.06.004

Shokri-Kojori, E., Tomasi, D., Wiers, C. E., Wang, G.-J., & Volkow, N. D. (2017). Alcohol affects brain functional connectivity and its coupling with behavior: Greater effects in male heavy drinkers. *Molecular Psychiatry*, *22*(8), 1185–1195. https://doi.org/10.1038/mp.2016.25

Shokri-Kojori, E., Tomasi, D., Alipanahi, B., Wiers, C. E., Wang, G.-J., & Volkow, N. D. (2019). Correspondence between cerebral glucose metabolism and BOLD reveals relative power and cost in human brain. *Nature Communications*, *10*(1), 690. https://doi.org/10.1038/s41467-019-08546-x

Striano, P., Weber, Y. G., Toliat, M. R., Schubert, J., Leu, C., Chaimana, R., ... EPICURE Consortium. (2012). GLUT1 mutations are a rare cause of familial idiopathic generalized epilepsy. *Neurology*, *78*(8), 557–562. https://doi.org/10.1212/WNL.0b013e318247ff54

Suls, A., Dedeken, P., Goffin, K., Van Esch, H., Dupont, P., Cassiman, D., ... Van Paesschen, W. (2008). Paroxysmal exercise-induced dyskinesia and epilepsy is due to mutations in SLC2A1, encoding the glucose transporter GLUT1. *Brain: A Journal of Neurology*, *131*(Pt 7), 1831–1844. https://doi.org/10.1093/brain/awn113

Suls, A., Mullen, S. A., Weber, Y. G., Verhaert, K., Ceulemans, B., Guerrini, R., ... Scheffer, I. E. (2009). Early-onset absence epilepsy caused by mutations in the glucose transporter GLUT1. *Annals of Neurology*, *66*(3), 415–419. https://doi.org/10.1002/ana.21724

Tang, M., Gao, G., Rueda, C. B., Yu, H., Thibodeaux, D. N., Awano, T., ... Monani, U. R. (2017). Brain microvasculature defects and Glut1 deficiency syndrome averted by early repletion of the glucose transporter-1 protein. *Nature Communications*, *8*, 14152. https://doi.org/10.1038/ncomms14152

Terpstra, M., Moheet, A., Kumar, A., Eberly, L. E., Seaquist, E., & Öz, G. (2014). Changes in human brain glutamate concentration during hypoglycemia: Insights into cerebral adaptations in hypoglycemia-associated autonomic failure in type 1 diabetes. *Journal of Cerebral Blood Flow and Metabolism: Official Journal of the International Society of Cerebral Blood Flow and Metabolism*, *34*(5), 876–882. https://doi.org/10.1038/jcbfm.2014.32

Tomasi, D., Wang, G.-J., & Volkow, N. D. (2013). Energetic cost of brain functional connectivity. *Proceedings of the National Academy of Sciences of the United States of America*, *110*(33), 13642–13647. https://doi.org/10.1073/pnas.1303346110

Tzourio-Mazoyer, N., Landeau, B., Papathanassiou, D., Crivello, F., Etard, O., Delcroix, N., ... Joliot, M. (2002). Automated anatomical labeling of activations in SPM using a macroscopic anatomical parcellation of the MNI MRI single-subject brain. *NeuroImage*, *15*(1), 273–289. https://doi.org/10.1006/nimg.2001.0978

van de Ven, K. C. C., Tack, C. J., Heerschap, A., van der Graaf, M., & de Galan, B. E. (2013). Patients with type 1 diabetes exhibit altered cerebral metabolism during hypoglycemia. *The Journal of Clinical Investigation*, *123*(2), 623–629. https://doi.org/10.1172/JCI62742

Vaudano, A. E., Olivotto, S., Ruggieri, A., Gessaroli, G., De Giorgis, V., Parmeggiani, A., ... Meletti, S. (2017). Brain correlates of spike and wave discharges in GLUT1 deficiency syndrome. *NeuroImage. Clinical*, *13*, 446–454. https://doi.org/10.1016/j.nicl.2016.12.026

Verrotti, A., D'Egidio, C., Agostinelli, S., & Gobbi, G. (2012). Glut1 deficiency: When to suspect and how to diagnose? *European Journal of Paediatric Neurology: EJPN: Official Journal of the European Paediatric Neurology Society*, *16*(1), 3–9. https://doi.org/10.1016/j.ejpn.2011.09.005

Vincent, J. L., Kahn, I., Snyder, A. Z., Raichle, M. E., & Buckner, R. L. (2008). Evidence for a frontoparietal control system revealed by intrinsic functional connectivity. *Journal of Neurophysiology*, *100*(6), 3328–3342. https://doi.org/10.1152/jn.90355.2008

Vincent, J. L., Snyder, A. Z., Fox, M. D., Shannon, B. J., Andrews, J. R., Raichle, M. E., & Buckner, R. L. (2006). Coherent spontaneous activity identifies a hippocampal-parietal memory network. *Journal of Neurophysiology*, *96*(6), 3517–3531. https://doi.org/10.1152/jn.00048.2006

Volkow, N. D., Wang, G.-J., Shokri Kojori, E., Fowler, J. S., Benveniste, H., & Tomasi, D. (2015). Alcohol decreases baseline brain glucose metabolism more in heavy drinkers than controls but has no effect on stimulation-induced metabolic increases. *The Journal of Neuroscience: The Official Journal of the Society for Neuroscience*, *35*(7), 3248–3255. https://doi.org/10.1523/JNEUROSCI.4877-14.2015

Wieloch, T. (1985). Hypoglycemia-induced neuronal damage prevented by an N-methyl-D-aspartate antagonist. *Science (New York, N.Y.)*, *230* (4726), 681–683.

Wilke, M., Schmithorst, V. J., & Holland, S. K. (2003). Normative pediatric brain data for spatial normalization and segmentation differs from standard adult data. *Magnetic Resonance in Medicine*, *50*(4), 749–757. https://doi.org/10.1002/mrm.10606

Yang, H., Wang, D., Engelstad, K., Bagay, L., Wei, Y., Rotstein, M., ... De Vivo, D. C. (2011). Glut1 deficiency syndrome and erythrocyte glucose uptake assay. *Annals of Neurology*, *70*(6), 996–1005. https://doi.org/10.1002/ana.22640

SUPPORTING INFORMATION

Additional supporting information may be found online in the Supporting Information section at the end of this article.